Arch Appl Mech (2019) 89:1885–1897
https://doi.org/10.1007/s00419-019-01549-6

ORIGINAL

Salamat Ullah · Haiyang Wang · Xinran Zheng · Jinghui Zhang · Yang Zhong · Rui Li

New analytic buckling solutions of moderately thick clamped rectangular plates by a straightforward finite integral transform method

Received: 15 January 2019 / Accepted: 6 April 2019 / Published online: 15 April 2019

Abstract A first endeavor is made in this paper to explore new analytic buckling solutions of moderately thick rectangular plates by a straightforward double finite integral transform method, with focus on typical non-Lévy-type fully clamped plates that are not easy to solve in a rigorous way by the other analytic methods. Solving the governing higher-order partial differential equations with prescribed boundary conditions is elegantly reduced to processing four sets of simultaneous linear equations, the existence of nonzero solutions of which determines the buckling loads and associated mode shapes. Both numerical and graphical results confirm the validity and accuracy of the developed method and solutions by favorable comparison with the literature and finite element analysis. The succinct but effective technique presented in this study can provide an easy-to-implement theoretical tool to seek more analytic solutions of complex boundary value problems.

Keywords Analytic solution · Thick plate · Buckling · Finite integral transform method

1 Introduction

The buckling analysis of moderately thick plates is an important research topic owing to its broad applications in numerous engineering fields such as civil, mechanical, marine and aerospace engineering. Representative practical examples include rigid pavements, aircraft wings, wallboards of the launch vehicles, etc., where the load carrying plate structures must endure enough compressive forces such that buckling of the structures, which may cause premature failure, is avoided. Obviously, predicting the buckling loads of such structures is indispensable for both the structural design and safety evaluation. To conduct the buckling analysis of plates, a series of theories have been developed, among which the classical plate theory (CPT) [1] is the simplest one that is usually used for thin plates by ignoring through-thickness shear effect. However, for moderately thick plates, the CPT underestimates deflections and overestimates buckling loads and natural frequencies. In order to overcome the limitations of the CPT, Reissner [2] and Mindlin [3] proposed the most commonly used shear deformation plate theories, both of which take the effect of transverse shear deformation into account. With the shear deformation theories, many studies have been reported to investigate the bending, vibration and

S. Ullah · J. Zhang · Y. Zhong
Faculty of Infrastructure Engineering, Dalian University of Technology, Dalian 116024, China

H. Wang · X. Zheng · R. Li (✉)
State Key Laboratory of Structural Analysis for Industrial Equipment, Department of Engineering Mechanics, and International Research Center for Computational Mechanics, Dalian University of Technology, Dalian 116024, China
E-mail: ruili@dlut.edu.cn

R. Li
State Key Laboratory of Nonlinear Mechanics, Institute of Mechanics, Chinese Academy of Sciences, Beijing 100190, China

buckling behavior of thick plates with different combinations of boundary constraints, loading conditions and material properties [4–7].

Some recent publications are reviewed here to reveal recent progresses in the field. Ghannadpour et al. [8] used an exact finite strip for the buckling and post-buckling analysis of thick plates; the strip was assumed to be simply supported at the loaded ends. Jafari and Azhari [9] presented a simple hp-cloud meshless method for the stability analysis of thick plates with various shapes. Civalek [10] applied an effective discrete singular convolution method for the three-dimensional static, buckling and vibration analyses of thick rectangular plates with clamped and simply supported boundary conditions. Bui et al. [11] proposed an elegant robust mesh-free moving Kriging interpolation method incorporating the shear-locking elimination technique for buckling analysis of thick plates. Bodaghi and Saidi [12] formulated a successful accurate thermal buckling analysis of Lévy-type thick functionally graded rectangular plates by decoupling the stability equations into two independent ones. Nazarimofrad et al. [13] successfully analyzed the buckling of a Lévy-type rotationally restrained orthotropic rectangular thick plate resting on a Pasternak elastic foundation by the Rayleigh–Ritz method. Yiotis and Katsikadelis [14] developed a straightforward meshless analog equation method for buckling analysis of thick plates resting on Pasternak-type elastic foundation. Recently, Li et al. [15–17] developed a novel symplectic superposition method for bending, buckling and free vibration of rectangular plates under different boundary conditions, which was a combination of the superposition method and symplectic elasticity approach developed by Yao et al. [18], Lim et al. [19], Lim [20] and Lim and Xu [21].

While many important achievements have been made, the research on plate buckling problems is still prosperous. One of the major concerns is on seeking new succinct but effective analytic techniques to solve some difficult plate buckling problems. In this context, a straightforward finite integral transform method has been developed in recent years by Li et al. [22], Tian et al. [23], and Zhang et al. [24] for bending of clamped thin plates and free thick plates as well as vibration of rotationally restrained thin plates. The method has also been adopted by Nwoji et al. [25] and Mama et al. [26] for bending and buckling of simply supported thin plates. The main advantage of the method is that it offers a simple general approach to handling a class of complex boundary value problems (BVPs) of higher-order partial differential equations (PDEs) represented by the plate problems, which provides an easy-to-implement tool for exploring more analytic solutions. However, there have been no reports on the use of the finite integral transform method for buckling analysis of thick plates, as far as the authors know.

This study presents a first endeavor to extend the double finite integral transform method to analytically solving the buckling problems of rectangular Mindlin plates, with focus on typical non-Lévy-type fully clamped plates that are not easy to solve in a rigorous way by the other analytic methods. Via the integral transform, solving the PDEs governing the bucking of a thick plate reduces to solving a system of linear algebraic equations. The analytic buckling load solutions are then readily determined by the existence of nonzero solutions of the system of equations. The analytic mode shape solutions can be further obtained. The numerical examples for the plates with different thickness-to-width and length-to-width ratios subjected to both uniaxial and biaxial compressive loads are given as the benchmark results, whose validity is well confirmed by satisfactory agreement with available solutions as well as the refined finite element analysis (FEA). Good convergence of the present solutions is also shown by the numerical results obtained by taking different numbers of series terms.

2 Governing equations and finite integral transform solutions for the buckling of Mindlin plates

2.1 Governing equations

Figure 1 illustrates a moderately thick rectangular plate in the *xoy* coordinate system, with a and b being the length and width of the plate in the x and y directions, and h the plate thickness in the z direction. According to Mindlin's first-order shear deformation theory, the governing buckling equations of the plate can be expressed as [27]

$$\begin{aligned}
&\frac{\partial^2 W}{\partial x^2}+\frac{\partial^2 W}{\partial y^2}-\frac{\partial \varphi_x}{\partial x}-\frac{\partial \varphi_y}{\partial y}+\frac{N_x}{C}\frac{\partial^2 W}{\partial x^2}+\frac{N_y}{C}\frac{\partial^2 W}{\partial y^2}=0\\
&\frac{\partial^2 \varphi_x}{\partial x^2}+\frac{1-\mu}{2}\frac{\partial^2 \varphi_x}{\partial y^2}+\frac{1+\mu}{2}\frac{\partial^2 \varphi_y}{\partial x\partial y}+\frac{C}{D}\left(\frac{\partial W}{\partial x}-\varphi_x\right)=0\\
&\frac{\partial^2 \varphi_y}{\partial y^2}+\frac{1-\mu}{2}\frac{\partial^2 \varphi_y}{\partial x^2}+\frac{1+\mu}{2}\frac{\partial^2 \varphi_x}{\partial x\partial y}+\frac{C}{D}\left(\frac{\partial W}{\partial y}-\varphi_y\right)=0
\end{aligned} \tag{1}$$

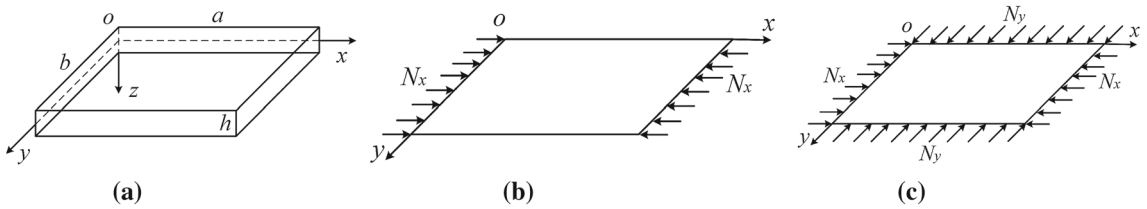

Fig. 1 Schematic illustrations of **a** a clamped Mindlin Plate, **b** the plate under uniaxial in-plane compression in the x direction, and **c** the plate under biaxial compression in both the x and y directions

where W is the transverse deflection of the plate, φ_x and φ_y are the rotations of the normal to the mid-surface about the y and x coordinates, N_x and N_y are the in-plane edge loads per unit length along the x and y coordinates; $C = sGh$ is the shear stiffness, with s being the shear correction factor (= 5/6 in this study), G the shear modulus satisfying $G = E/[2\,(1+\mu)]$ in which E is the Young's modulus and μ the Poisson's ratio; $D = Eh^3/\left[12\left(1-\mu^2\right)\right]$ is the flexural stiffness.

For a fully clamped plate under consideration, all the displacements are restricted at each edge. Therefore, the following boundary conditions hold: $W|_{x=0,a} = 0$, $\varphi_x|_{x=0,a} = 0$, $\varphi_y|_{x=0,a} = 0$, and $W|_{y=0,b} = 0$, $\varphi_x|_{y=0,b} = 0$, $\varphi_y|_{y=0,b} = 0$.

2.2 Finite integral transform

In order to solve Eq. (1), the double finite integral transforms are defined in "Appendix A" for W, φ_x and φ_y. The inversion gives

$$\begin{aligned} W\,(x,\,y) &= \frac{4}{ab}\sum_{m=1}^{\infty}\sum_{n=1}^{\infty} W^{\mathrm{SS}}\sin\left(\alpha_m x\right)\sin\left(\beta_n y\right) \\ \varphi_x\,(x,\,y) &= \frac{2}{ab}\sum_{m=0}^{\infty}\sum_{n=1}^{\infty} \varepsilon_m\varphi_x^{\mathrm{CS}}\cos\left(\alpha_m x\right)\sin\left(\beta_n y\right) \\ \varphi_y\,(x,\,y) &= \frac{2}{ab}\sum_{m=1}^{\infty}\sum_{n=0}^{\infty} \varepsilon_m\varphi_y^{\mathrm{SC}}\sin\left(\alpha_m x\right)\cos\left(\beta_n y\right) \end{aligned} \tag{2}$$

where $\alpha_m = m\pi/a$, $\beta_n = n\pi/b$, and $\varepsilon_m\,(\varepsilon_n) = \begin{cases} 1 \text{ for } m\,(n) = 0 \\ 2 \text{ for } m\,(n) = 1,\ 2,\ \ldots \end{cases}$; the superscripts "SS", "CS" and "SC" represent the double sine, cosine-sine and sine-cosine integral transforms with respect to variables x and y.

Applying the integral transforms to each term of Eq. (1), the following relationships are derived in sequence:

$$\int_0^a\int_0^b \frac{\partial^2 W}{\partial x^2}\sin\left(\alpha_m x\right)\sin\left(\beta_n y\right)\mathrm{d}x\mathrm{d}y = -\alpha_m^2 W^{\mathrm{SS}} - \alpha_m\int_0^b\left[(-1)^m\ W|_{x=a} - \ W|_{x=0}\right]\sin\left(\beta_n y\right)\mathrm{d}y$$

$$\int_0^a\int_0^b \frac{\partial^2 W}{\partial y^2}\sin\left(\alpha_m x\right)\sin\left(\beta_n y\right)\mathrm{d}x\mathrm{d}y = -\beta_n^2 W^{\mathrm{SS}} - \beta_n\int_0^a\left[(-1)^n\ W|_{y=b} - \ W|_{y=0}\right]\sin\left(\alpha_m x\right)\mathrm{d}x$$

$$\int_0^a\int_0^b \frac{\partial \varphi_x}{\partial x}\sin\left(\alpha_m x\right)\sin\left(\beta_n y\right)\mathrm{d}x\mathrm{d}y = -\alpha_m\varphi_x^{\mathrm{CS}}$$

$$\int_0^a\int_0^b \frac{\partial \varphi_y}{\partial y}\sin\left(\alpha_m x\right)\sin\left(\beta_n y\right)\mathrm{d}x\mathrm{d}y = -\beta_n\varphi_y^{\mathrm{SC}}$$

$$\int_0^a\int_0^b \frac{\partial^2\varphi_x}{\partial x^2}\cos(\alpha_m x)\sin(\beta_n y)\,\mathrm{d}x\mathrm{d}y = -\alpha_m^2\varphi_x^{\mathrm{cs}} + \int_0^b\left[(-1)^m\left.\frac{\partial\varphi_x}{\partial x}\right|_{x=a} - \left.\frac{\partial\varphi_x}{\partial x}\right|_{x=0}\right]\sin(\beta_n y)\,\mathrm{d}y$$

$$\int_0^a\int_0^b \frac{\partial^2\varphi_x}{\partial y^2}\cos(\alpha_m x)\sin(\beta_n y)\,\mathrm{d}x\mathrm{d}y = -\beta_n^2\varphi_x^{\mathrm{cs}} - \beta_n\int_0^a\left[(-1)^n\left.\varphi_x\right|_{y=b} - \left.\varphi_x\right|_{y=0}\right]\cos(\alpha_m x)\,\mathrm{d}x$$

$$\int_0^a\int_0^b \frac{\partial^2\varphi_y}{\partial x\partial y}\cos(\alpha_m x)\sin(\beta_n y)\,\mathrm{d}x\mathrm{d}y = -\alpha_m\beta_n\varphi_y^{\mathrm{sc}} - \beta_n\int_0^b\left[(-1)^m\left.\varphi_y\right|_{x=a} - \left.\varphi_y\right|_{x=0}\right]\cos(\beta_n y)\,\mathrm{d}y$$

$$\int_0^a\int_0^b \frac{\partial W}{\partial x}\cos(\alpha_m x)\sin(\beta_n y)\,\mathrm{d}x\mathrm{d}y = \alpha_m W^{\mathrm{ss}} + \int_0^b\left[(-1)^m\left.W\right|_{x=a} - \left.W\right|_{x=0}\right]\sin(\beta_n y)\,\mathrm{d}y$$

$$\int_0^a\int_0^b \frac{\partial^2\varphi_y}{\partial y^2}\sin(\alpha_m x)\cos(\beta_n y)\,\mathrm{d}x\mathrm{d}y = -\beta_n^2\varphi_y^{\mathrm{sc}} + \int_0^a\left[(-1)^n\left.\frac{\partial\varphi_y}{\partial y}\right|_{y=b} - \left.\frac{\partial\varphi_y}{\partial y}\right|_{y=0}\right]\sin(\alpha_m x)\,\mathrm{d}x$$

$$\int_0^a\int_0^b \frac{\partial^2\varphi_y}{\partial x^2}\sin(\alpha_m x)\cos(\beta_n y)\,\mathrm{d}x\mathrm{d}y = -\alpha_m^2\varphi_y^{\mathrm{sc}} - \alpha_m\int_0^b\left[(-1)^m\left.\varphi_y\right|_{x=a} - \left.\varphi_y\right|_{x=0}\right]\cos(\beta_n y)\,\mathrm{d}y$$

$$\int_0^a\int_0^b \frac{\partial^2\varphi_x}{\partial x\partial y}\sin(\alpha_m x)\cos(\beta_n y)\,\mathrm{d}x\mathrm{d}y = -\alpha_m\beta_n\varphi_x^{\mathrm{cs}} - \alpha_m\int_0^a\left[(-1)^n\left.\varphi_x\right|_{y=b} - \left.\varphi_x\right|_{y=0}\right]\cos(\alpha_m x)\,\mathrm{d}x$$

$$\int_0^a\int_0^b \frac{\partial W}{\partial y}\sin(\alpha_m x)\cos(\beta_n y)\,\mathrm{d}x\mathrm{d}y = \beta_n W^{\mathrm{ss}} + \int_0^a\left[(-1)^n\left.W\right|_{y=b} - \left.W\right|_{y=0}\right]\sin(\alpha_m x)\,\mathrm{d}x \tag{3}$$

Using Eq. (3), the integral transform of Eq. (1) yields

$$\begin{aligned}
&\alpha_m^2 W^{\mathrm{ss}} + \beta_n^2 W^{\mathrm{ss}} - \alpha_m\varphi_x^{\mathrm{cs}} - \beta_n\varphi_y^{\mathrm{sc}}\\
&+\alpha_m\int_0^b\left[(-1)^m\left.W\right|_{x=a} - \left.W\right|_{x=0}\right]\sin(\beta_n y)\,\mathrm{d}y\\
&+\beta_n\int_0^a\left[(-1)^n\left.W\right|_{y=b} - \left.W\right|_{y=0}\right]\sin(\alpha_m x)\,\mathrm{d}x\\
&+\frac{N_x}{C}\left\{\alpha_m^2 W^{\mathrm{ss}} + \alpha_m\int_0^b\left[(-1)^m\left.W\right|_{x=a} - \left.W\right|_{x=0}\right]\sin(\beta_n y)\,\mathrm{d}y\right\}\\
&+\frac{N_y}{C}\left\{\beta_n^2 W^{\mathrm{ss}} + \beta_n\int_0^a\left[(-1)^n\left.W\right|_{y=b} - \left.W\right|_{y=0}\right]\sin(\alpha_m x)\,\mathrm{d}x\right\} = 0
\end{aligned} \tag{4}$$

$$\begin{aligned}
&\alpha_m^2\varphi_x^{\mathrm{cs}} - \int_0^b\left[(-1)^m\left.\frac{\partial\varphi_x}{\partial x}\right|_{x=a} - \left.\frac{\partial\varphi_x}{\partial x}\right|_{x=0}\right]\sin(\beta_n y)\,\mathrm{d}y\\
&+\frac{1-\mu}{2}\left\{\beta_n^2\varphi_x^{\mathrm{cs}} + \beta_n\int_0^a\left[(-1)^n\left.\varphi_x\right|_{y=b} - \left.\varphi_x\right|_{y=0}\right]\cos(\alpha_m x)\,\mathrm{d}x\right\}
\end{aligned}$$

$$+\frac{1+\mu}{2}\left\{\alpha_m\beta_n\varphi_y^{\mathrm{sc}}+\beta_n\int_0^b\left[(-1)^m\ \varphi_y|_{x=a}-\varphi_y|_{x=0}\right]\cos(\beta_n y)\,\mathrm{d}y\right\}$$
$$+\frac{C}{D}\left\{\varphi_x-\alpha_m W^{\mathrm{ss}}-\int_0^b\left[(-1)^m\ W|_{x=a}-W|_{x=0}\right]\sin(\beta_n y)\,\mathrm{d}y\right\}=0 \tag{5}$$

$$\beta_n^2\varphi_y^{\mathrm{sc}}-\int_0^a\left[(-1)^n\ \frac{\partial\varphi_y}{\partial y}\bigg|_{y=b}-\frac{\partial\varphi_y}{\partial y}\bigg|_{y=0}\right]\sin(\alpha_m x)\,\mathrm{d}x$$
$$+\frac{1-\mu}{2}\left\{\alpha_m^2\varphi_y^{\mathrm{sc}}+\alpha_m\int_0^b\left[(-1)^m\ \varphi_y|_{x=a}-\varphi_y|_{x=0}\right]\cos(\beta_n y)\,\mathrm{d}y\right\}$$
$$+\frac{1+\mu}{2}\left\{\alpha_m\beta_n\varphi_x^{\mathrm{cs}}+\alpha_m\int_0^a\left[(-1)^n\ \varphi_x|_{y=b}-\varphi_x|_{y=0}\right]\cos(\alpha_m x)\,\mathrm{d}x\right\}$$
$$+\frac{C}{D}\left\{\varphi_y-\beta_n W^{\mathrm{ss}}-\int_0^a\left[(-1)^n\ W|_{y=b}-W|_{y=0}\right]\sin(\alpha_m x)\,\mathrm{d}x\right\}=0 \tag{6}$$

By applying the boundary conditions $W|_{x=0,a}=0$, $W|_{y=0,b}=0$, $\varphi_y|_{x=0,a}=0$ and $\varphi_x|_{y=0,b}=0$, Eqs. (4)–(6) give

$$\alpha_m\varphi_x^{\mathrm{cs}}+\beta_n\varphi_y^{\mathrm{sc}}-\left(\alpha_m^2+\beta_n^2+\frac{N_x}{C}\alpha_m^2+\frac{N_y}{C}\beta_n^2\right)W^{\mathrm{ss}}=0 \tag{7}$$

$$\frac{C}{D}\alpha_m W^{\mathrm{ss}}-\left(\alpha_m^2+\frac{1-\mu}{2}\beta_n^2+\frac{C}{D}\right)\varphi_x^{\mathrm{cs}}-\frac{1+\mu}{2}\alpha_m\beta_n\varphi_y^{\mathrm{sc}}=(-1)^{m+1}K_n+L_n \tag{8}$$

$$\frac{C}{D}\beta_n W^{\mathrm{ss}}-\frac{1+\mu}{2}\alpha_m\beta_n\varphi_x^{\mathrm{cs}}-\left(\beta_n^2+\frac{1-\mu}{2}\alpha_m^2+\frac{C}{D}\right)\varphi_y^{\mathrm{sc}}=(-1)^{n+1}I_m+J_m \tag{9}$$

where

$$I_m=\int_0^a\frac{\partial\varphi_y}{\partial y}\bigg|_{y=b}\sin(\alpha_m x)\,\mathrm{d}x$$
$$J_m=\int_0^a\frac{\partial\varphi_y}{\partial y}\bigg|_{y=0}\sin(\alpha_m x)\,\mathrm{d}x$$
$$K_n=\int_0^b\frac{\partial\varphi_x}{\partial x}\bigg|_{x=a}\sin(\beta_n y)\,\mathrm{d}y$$
$$L_n=\int_0^b\frac{\partial\varphi_x}{\partial x}\bigg|_{x=0}\sin(\beta_n y)\,\mathrm{d}y \tag{10}$$

Assume $N_x=s_1N$ and $N_y=s_2N$, where s_1 and $s_2$are the scaling parameters for the in-plane loads N in the x and y directions, respectively. From Eqs. (7)–(9), the following matrix form is obtained for the expression of W^{ss}, $\varphi_x^{\mathrm{cs}}$and φ_y^{sc}:

$$\begin{Bmatrix}W^{\mathrm{ss}}\\ \varphi_x^{\mathrm{cs}}\\ \varphi_y^{\mathrm{sc}}\end{Bmatrix}=\mathbf{T}_{3\times3}\begin{Bmatrix}0\\ (-1)^{m+1}K_n+L_n\\ (-1)^{n+1}I_m+J_m\end{Bmatrix} \tag{11}$$

where $\mathbf{T}_{3\times3}$ is the coefficient matrix, the elements of which, T_{ij} $(i,\ j=1,2,3)$, are shown in "Appendix B".

2.3 Analytic buckling solutions

The remaining boundary conditions that have not been satisfied include $\varphi_x|_{x=0,a} = 0$ and $\varphi_y\big|_{y=0,b} = 0$, which require, according to Eq. (2),

$$\begin{aligned}
&\sum_{n=1}^{\infty}\left[\frac{2}{ab}\sum_{m=0}^{\infty}\varepsilon_m\varphi_x^{\mathrm{cs}}\cos(\alpha_m x)\big|_{x=0,a}\right]\sin(\beta_n y)=0\\
&\sum_{m=1}^{\infty}\left[\frac{2}{ab}\sum_{n=0}^{\infty}\varepsilon_n\varphi_y^{\mathrm{sc}}\cos(\beta_n y)\Big|_{y=0,b}\right]\sin(\alpha_m x)=0
\end{aligned}\tag{12}$$

Substitute Eq. (11) into Eq. (12), in view of the orthogonality of the sine series, we finally obtain

$$\begin{aligned}
&2\sum_{m=1}(-1)^n T_{23}I_m - 2\sum_{m=1}T_{23}J_m\\
&+\left[T_{22}(m=0)+2\sum_{m=1}(-1)^m T_{22}\right]K_n-\left[T_{22}(m=0)+2\sum_{m=1}T_{22}\right]L_n=0
\end{aligned}\tag{13}$$

and

$$\begin{aligned}
&2\sum_{m=1}(-1)^{m+n} T_{23}I_m - 2\sum_{m=1}(-1)^m T_{23}J_m\\
&+\left[T_{22}(m=0)+2\sum_{m=1}T_{22}\right]K_n-\left[T_{22}(m=0)+2\sum_{m=1}(-1)^m T_{22}\right]L_n=0
\end{aligned}\tag{14}$$

for $n = 1, 2, 3, \ldots$, and

$$\begin{aligned}
&\left[T_{33}(n=0)+2\sum_{n=1}(-1)^n T_{33}\right]I_m-\left[T_{33}(n=0)+2\sum_{n=1}T_{33}\right]J_m\\
&+2\sum_{n=1}(-1)^m T_{23}K_n-2\sum_{n=1}T_{23}L_n=0
\end{aligned}\tag{15}$$

and

$$\begin{aligned}
&\left[T_{33}(n=0)+2\sum_{n=1}T_{33}\right]I_m-\left[T_{33}(n=0)+2\sum_{n=1}(-1)^n T_{33}\right]J_m\\
&+2\sum_{n=1}(-1)^{m+n} T_{23}K_n-2\sum_{n=1}(-1)^n T_{23}L_n=0
\end{aligned}\tag{16}$$

for $m = 1, 2, 3, \ldots$.

Equations (13)–(16) are four sets of simultaneous linear equations with respect to the constants I_m, J_m, K_n and L_n $(m, n = 1, 2, 3, \ldots)$. A finite number of equations are treated in practice with the same number of constants. For example, Eqs. (13) and (14) are taken for $n = 1, 2, 3, \ldots, N$, and Eqs. (15) and (16) are taken for $m = 1, 2, 3, \ldots, M$, where M and N represent any positive integers; meanwhile, instead of ∞, M and N are taken in Eqs. (13)–(16) as the upper limits of summations with respect to I_m and J_m, and K_n and L_n, respectively. Accordingly, $2M + 2N$ equations are formed with respect to I_m, J_m, K_n and L_n $(m = 1, 2, 3, \ldots, M; n = 1, 2, 3, \ldots, N)$. The existence of nonzero solutions requires that the determinant of the coefficient matrix of the above sets of equations be zero; this leads to the equation of buckling loads, substituting one of the roots (i.e., a buckling load solution) back to the sets of equations yields nonzero solutions for the constants. By substituting the above constant solutions into Eq. (11), then into Eq. (2), we finally get the analytic mode shape solutions of the plate corresponding to the buckling load.

Table 1 Buckling factors, $Nb^2/(D\pi^2)$, for CCCC Mindlin plates subjected to uniaxial compression ($S_1 = -1$, $S_2 = 0$)

h/*b*	*a*/*b*	Method	Mode					
			1st	2nd	3rd	4th	5th	6th
0.05	0.5	Present	17.223	27.852	27.973	33.993	45.250	45.389
		FEM	17.204	27.789	27.950	33.891	45.053	45.351
		Xiang [30]	17.222					
		Teo and Liew [29]	16.954					
	1	Present	9.5595	10.772	17.357	22.152	22.615	22.945
		FEM	9.5517	10.760	17.342	22.106	22.598	22.887
		Xiang [30]	9.5588					
		Teo and Liew [29]	9.5514					
	1.5	Present	7.9436	8.7508	12.773	13.258	18.064	20.713
		FEM	7.9359	8.7420	12.761	13.249	18.043	20.698
		Xiang [30]	7.9431					
		Teo and Liew [29]	7.9931					
	2	Present	7.4874	7.7010	9.7026	10.725	13.835	15.710
		FEM	7.4799	7.6939	9.6941	10.715	13.823	15.698
		Xiang [30]	7.4870					
		Teo and Liew [29]	7.5923					
	2.5	Present	7.2306	7.2677	8.7498	9.3115	11.402	11.943
		FEM	7.2238	7.2603	8.7412	9.3032	11.394	11.932
		Xiang [30]	7.2304					
		Teo and Liew [29]	7.5126					
0.1	0.5	Present	13.027	17.356	19.580	20.730	23.515	25.802
		FEM	12.966	17.301	19.467	20.560	23.467	25.751
		Xiang [30]	13.026					
		Teo and Liew [29]	12.476					
	1	Present	8.2921	8.9031	13.181	15.430	16.590	16.623
		FEM	8.2583	8.8595	13.140	15.388	16.496	16.521
		Xiang [30]	8.2917					
		Teo and Liew [29]	8.1391					
	1.5	Present	6.9612	7.4943	10.251	10.881	13.996	14.604
		FEM	6.9255	7.4567	10.210	10.848	13.968	14.567
		Xiang [30]	6.9608					
		Teo and Liew [29]	6.8891					
	2	Present	6.5739	6.7545	8.3376	8.8763	10.959	12.014
		FEM	6.5382	6.7201	8.3028	8.8378	10.921	11.978
		Xiang [30]	6.5736					
		Teo and Liew [29]	6.5668					
	2.5	Present	6.3909	6.3917	7.5415	7.9541	9.6662	9.6948
		FEM	6.3563	6.3570	7.5052	7.9183	9.6343	9.6573
		Xiang [30]	6.3908					
		Teo and Liew [29]	6.5866					
0.15	0.5	Present	9.2884	10.702	12.601	12.674	13.050	13.478
		FEM	9.2251	10.654	12.546	12.565	13.016	13.457
		Xiang [30]	9.2881					
		Teo and Liew [29]	8.8623					
	1	Present	6.7597	6.9479	9.4409	10.122	11.481	11.526
		FEM	6.7077	6.8900	9.4048	10.084	11.372	11.421
		Xiang [30]	6.7595					
		Teo and Liew [29]	6.5449					
	1.5	Present	5.8014	6.0789	7.7539	8.1645	9.8264	9.9353
		FEM	5.7414	6.0203	7.7070	8.1233	9.7940	9.9107
		Xiang [30]	5.8012					
		Teo and Liew [29]	5.6601					
	2	Present	5.5015	5.6246	6.7637	6.9321	8.1958	8.6168
		FEM	5.4396	5.5637	6.7122	6.8818	8.1559	8.5800
		Xiang [30]	5.5013					
		Teo and Liew [29]	5.4254					
	2.5	Present	5.3620	5.3820	6.1724	6.3965	7.4219	7.5844
		FEM	5.2996	5.3196	6.1166	6.3425	7.3774	7.5403
		Xiang [30]	5.3629					
		Teo and Liew [29]	5.5132					
0.2	0.5	Present	6.6167	7.0073	8.0412	8.0985	8.1681	8.4641
		FEM	6.5743	6.9737	8.0242	8.0878	8.1415	8.4921
		Xiang [30]	6.6166					

Table 1 continued

h/*b*	*a*/*b*	Method	Mode					
			1st	2nd	3rd	4th	5th	6th
		Teo and Liew [29]	6.3903					
	1	Present	5.3157	5.3350	6.7066	6.8482	7.5767	7.6554
		FEM	5.2664	5.2821	6.6871	6.8206	7.5682	7.6392
		Xiang [30]	5.3156					
		Teo and Liew [29]	5.1166					
	1.5	Present	4.7157	4.8280	5.7995	5.9760	6.7556	6.8400
		FEM	4.6514	4.7673	5.7618	5.9407	6.7334	6.8215
		Xiang [30]	4.7156					
		Teo and Liew [29]	4.5691					
	2	Present	4.5027	4.5684	5.3156	5.3248	6.0701	6.1776
		FEM	4.4337	4.5006	5.2664	5.2792	6.0404	6.1485
		Xiang [30]	4.5026					
		Teo and Liew [29]	4.4127					
	2.5	Present	4.4027	4.4242	4.9388	5.0232	5.6105	5.7158
		FEM	4.3314	4.3517	4.8817	4.9703	5.5726	5.6778
		Xiang [30]	4.4033					
		Teo and Liew [29]	4.5269					

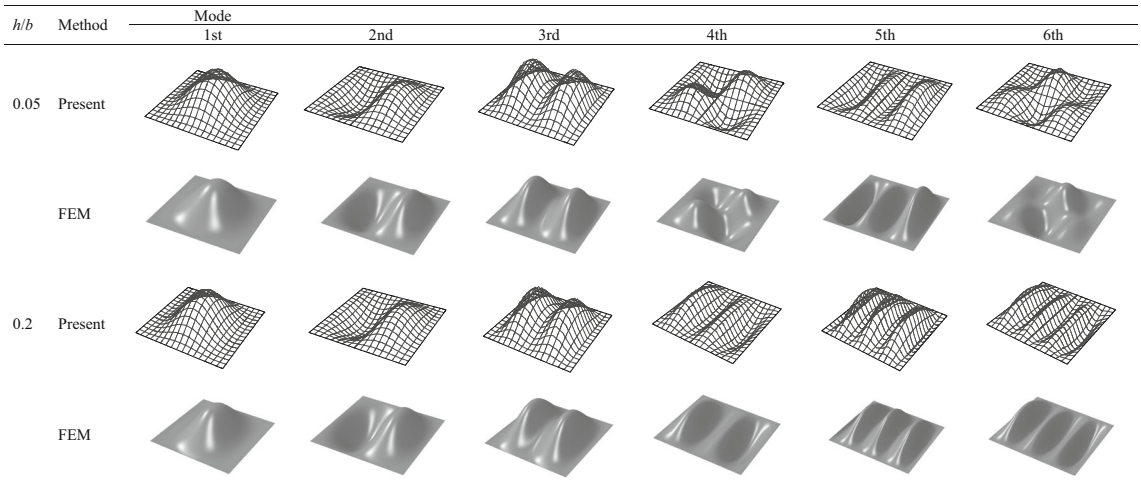

Fig. 2 First six buckling mode shapes of CCCC square plates subjected to uniaxial compression ($S_1 = -1$, $S_2 = 0$), with h/b= 0.05 and 0.2

3 Numerical and graphical results

Table 1 presents the non-dimensional finite integral transform solutions for the buckling loads, denoted by $Nb^2/(D\pi^2)$, of fully clamped thick plates with different geometric parameters subjected to uniaxial compression ($S_1 = -1$ and $S_2 = 0$). The results are listed for the aspect ratios being 0.5, 1, 1.5, 2 and 2.5 under the thickness-to-width ratios 0.05, 0.1, 0.15 and 0.2, respectively. The present results for the first six buckling modes are compared with the FEA by the commercial software ABAQUS [28] (with S4R shell element adopted) as well as numerical solutions from the literature [29,30] that only provide the lowest buckling loads. Good agreement is observed with those for comparison, especially with the refined FEA. The quantitative results show that increasing the thickness-to-width ratio decreases the buckling load and vice versa, which indicates that shear deformation plays an important role as a plate gets thicker. It is also found that the buckling load decreases as the aspect ratio increases. The buckling mode shapes for uniaxially compressed square plates with two different thickness-to-width ratios are plotted in Fig. 2, with good agreement observed with the FEA results.

Table 2 shows the buckling loads of fully clamped thick plates subjected to biaxial compression ($S_1 = -1$ and $S_2 = -1.5$). The solutions are presented in the same way as those in Table 1. The results are partly compared with the numerical solutions available from the literature [10,29] and are all compared with the

Table 2 Buckling factors for CCCC Mindlin plates subjected to biaxial compression ($S_1 = -1$, $S_2 = -1.5$)

h/*b*	*a*/*b*	Method	Mode					
			1st	2nd	3rd	4th	5th	6th
0.05	0.5	Present	12.049	12.381	14.432	17.486	21.705	25.077
		FEM	12.007	12.355	14.382	17.415	21.628	24.992
		Civalek [10]	11.8611					
		Teo and Liew [29]	11.862					
	1	Present	4.0593	6.2019	7.8559	9.3774	10.055	12.475
		FEM	4.0563	6.1963	7.8497	9.3596	10.047	12.446
		Civalek [10]	4.0561					
		Teo and Liew [29]	4.0358					
	1.5	Present	2.9608	4.3418	5.5048	6.6862	6.7993	8.7256
		FEM	2.9596	4.3387	5.5029	6.6795	6.7945	8.7215
		Civalek [10]	2.9541					
		Teo and Liew [29]	2.9537					
	2	Present	2.7196	3.3045	4.5229	5.3163	5.9018	6.3111
		FEM	2.7190	3.3027	4.5199	5.3155	5.8984	6.3070
	2.5	Present	2.6465	2.9257	3.5799	4.6287	5.2410	5.5857
		FEM	2.6462	2.9246	3.5778	4.6257	5.2405	5.5837
0.1	0.5	Present	8.8107	9.0933	10.304	11.359	13.002	14.400
		FEM	8.6858	8.9830	10.222	11.243	12.906	14.316
		Civalek [10]	8.4821					
		Teo and Liew [29]	8.4809					
	1	Present	3.6246	5.1466	6.5055	7.3422	7.6038	9.0391
		FEM	3.6103	5.1236	6.4793	7.2815	7.5755	8.9611
		Civalek [10]	3.5491					
		Teo and Liew [29]	3.5494					
	1.5	Present	2.7077	3.8598	4.6343	5.5074	5.7712	6.9488
		FEM	2.7020	3.8452	4.6257	5.4791	5.7501	6.9001
		Civalek [10]	2.6614					
		Teo and Liew [29]	2.6614					
	2	Present	2.5000	2.9979	4.0136	4.4927	4.9325	5.4229
		FEM	2.4970	2.9885	3.9988	4.4885	4.9168	5.4043
	2.5	Present	2.4376	2.6736	3.2323	4.1038	4.4359	4.6959
		FEM	2.4356	2.6675	3.2213	4.0891	4.4333	4.6862
0.15	0.5	Present	6.1556	6.2795	7.0646	7.2408	7.9056	8.2714
		FEM	6.0240	6.1511	6.9996	7.1637	7.8596	8.2266
		Civalek [10]	5.9042					
		Teo and Liew [29]	5.9035					
	1	Present	3.0899	4.0306	5.0732	5.4354	5.4377	6.2579
		FEM	3.0645	3.9974	5.0340	5.3648	5.4018	6.1825
		Civalek [10]	2.9784					
		Teo and Liew [29]	2.9794					
	1.5	Present	2.3769	3.2727	3.6767	4.2830	4.6192	5.2230
		FEM	2.3647	3.2461	3.6624	4.2407	4.5862	5.1603
		Civalek [10]	2.3007					
		Teo and Liew [29]	2.3011					
	2	Present	2.2068	2.6069	3.3953	3.5759	3.8882	4.4077
		FEM	2.1998	2.5878	3.3687	3.5681	3.8629	4.3707
	2.5	Present	2.1558	2.3447	2.7945	3.4676	3.5351	3.7211
		FEM	2.1513	2.3309	2.7727	3.4412	3.5303	3.7037
0.2	0.5	Present	4.2935	4.3897	4.8205	4.8255	5.1535	5.1973
		FEM	4.2548	4.2907	4.7745	4.8773	5.1351	5.1731
	1	Present	2.5692	3.1039	3.8812	3.9014	4.0089	4.3430
		FEM	2.5400	3.0712	3.8415	3.8734	3.9470	4.3217
	1.5	Present	2.0352	2.7080	2.8587	3.2822	3.5964	3.8945
		FEM	2.0185	2.6767	2.8426	3.2393	3.5623	3.8390
	2	Present	1.8987	2.2130	2.7859	2.8030	3.0108	3.3766
		FEM	1.8881	2.1873	2.7718	2.7765	2.9815	3.3309
	2.5	Present	1.8574	2.0065	2.3592	2.7562	2.8599	2.8916
		FEM	1.8501	1.9862	2.3306	2.7501	2.8290	2.8610

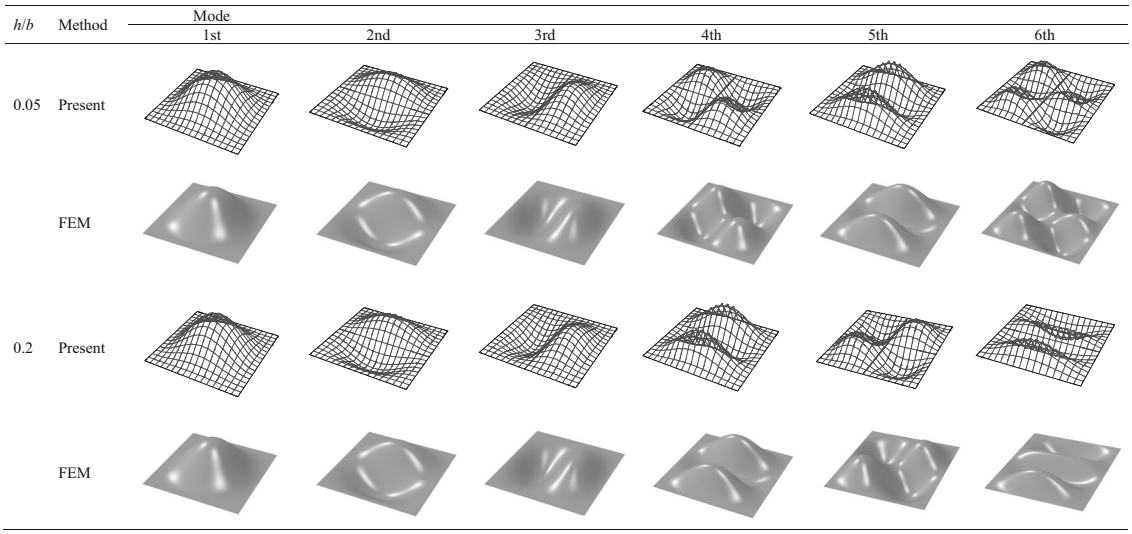

Fig. 3 First six buckling mode shapes of CCCC square plates subjected to biaxial compression ($S_1 = -1$, $S_2 = -1.5$), with h/b= 0.05 and 0.2

Table 3 Convergence study for buckling factors of CCCC Mindlin plates subjected to uniaxial compression

h/b	a/b	No. of series terms	Mode					
			1st	2nd	3rd	4th	5th	6th
0.05	0.5	20	17.228	27.859	27.980	34.001	45.259	45.399
		40	17.225	27.855	27.976	33.996	45.254	45.393
		60	17.224	27.854	27.974	33.995	45.252	45.391
		80	17.224	27.853	27.974	33.994	45.251	45.390
		100	**17.223**	**27.852**	**27.973**	**33.993**	**45.250**	**45.389**
		120	17.223	27.852	27.973	33.993	45.250	45.389
	2.5	20	7.2327	7.2698	8.7524	9.3142	11.405	11.947
		40	7.2314	7.2685	8.7508	9.3125	11.403	11.945
		60	7.2310	7.2680	8.7502	9.3120	11.402	11.944
		80	7.2307	7.2678	8.7500	9.3117	11.402	11.944
		100	**7.2306**	**7.2677**	**8.7498**	**9.3115**	**11.402**	**11.943**
		120	7.2306	7.2677	8.7498	9.3115	11.402	11.943
0.2	0.5	20	6.6171	7.0075	8.0414	8.0986	8.1681	8.4642
		40	6.6167	7.0074	8.0413	8.0986	8.1681	8.4641
		60	6.6168	7.0073	8.0412	8.0985	8.1681	8.4641
		80	**6.6167**	**7.0073**	**8.0412**	**8.0985**	**8.1681**	**8.4641**
		100	6.6167	7.0073	8.0412	8.0985	8.1681	8.4641
	2.5	20	4.4031	4.4247	4.9393	5.0236	5.6110	5.7163
		40	4.4028	4.4244	4.9390	5.0234	5.6107	5.7160
		60	4.4028	4.4243	4.9389	5.0233	5.6106	5.7159
		80	4.4027	4.4243	4.9389	5.0233	5.6106	5.7159
		100	**4.4027**	**4.4242**	**4.9388**	**5.0232**	**5.6105**	**5.7158**
		120	4.4027	4.4242	4.9388	5.0232	5.6105	5.7158

FEA. Again, good agreement is realized, which confirms the validity and accuracy of the present solutions. The buckling mode shapes for biaxially compressed square plates with two different thickness-to-width ratios are plotted in Fig. 3, where satisfactory agreement with the FEA is achieved.

Tables 3 and 4 show the convergence study of the solutions for plates under both uniaxial and biaxial compressions by taking extreme thickness-to-width ratios (0.05 and 0.2) and length-to-width ratios (0.5 and 2.5) as per Tables 1 and 2, with the convergent results marked in bold. The accuracy of five significant figures is attained by taking 100 series terms at most (e.g., $M = N = 100$) in our solution, which can be easily conducted on an ordinary personal computer. Accordingly, $M = N = 100$ has been adopted throughout this study.

Table 4 Convergence study for buckling factors of CCCC Mindlin plates subjected to biaxial compression.

h/*b*	*a*/*b*	No. of series terms	Mode					
			1st	2nd	3rd	4th	5th	6th
0.05	0.5	20	12.052	12.385	14.435	17.491	21.711	25.083
		40	12.050	12.383	14.433	17.488	21.707	25.080
		60	12.050	12.382	14.432	17.487	21.706	25.078
		80	12.049	12.382	14.432	17.487	21.706	25.078
		100	**12.049**	**12.381**	**14.432**	**17.486**	**21.705**	**25.077**
		120	12.049	12.381	14.432	17.486	21.705	25.077
	2.5	20	2.6474	2.9266	3.5810	4.6302	5.2426	5.5874
		40	2.6469	2.9260	3.5803	4.6293	5.2416	5.5863
		60	2.6467	2.9258	3.5801	4.6290	5.2413	5.5860
		80	2.6466	2.9258	3.5800	4.6289	5.2411	5.5858
		100	**2.6465**	**2.9257**	**3.5799**	**4.6287**	**5.2410**	**5.5857**
		120	2.6465	2.9257	3.5799	4.6287	5.2410	5.5857
0.2	0.5	20	4.2940	4.3899	4.8207	4.8256	5.1537	5.1975
		40	4.2937	4.3898	4.8206	4.8255	5.1536	5.1974
		60	4.2937	4.3898	4.8206	4.8255	5.1536	5.1974
		80	**4.2935**	**4.3897**	**4.8205**	**4.8255**	**5.1535**	**5.1973**
		100	4.2935	4.3897	4.8205	4.8255	5.1535	5.1973
	2.5	20	1.8578	2.0069	2.3596	2.7566	2.8603	2.8925
		40	1.8576	2.0067	2.3594	2.7563	2.8601	2.8918
		60	1.8575	2.0066	2.3593	2.7563	2.8600	2.8917
		80	1.8575	2.0065	2.3593	2.7562	2.8599	2.8917
		100	**1.8574**	**2.0065**	**2.3592**	**2.7562**	**2.8599**	**2.8916**
		120	1.8574	2.0065	2.3592	2.7562	2.8599	2.8916

4 Conclusions

The double finite integral transform method is extended to the buckling problems of rectangular thick plates. The solution procedure is conducted in a concise but rigorous way, which starts from the governing high-order PDEs. By satisfying some boundary conditions, the relationship is found between the displacements in the transform domain and the constants that are determined by the equations yielded by the remaining boundary conditions. The inversion of the integral transforms gives the analytic buckling solutions of the plates. Comprehensive buckling loads and mode shapes are obtained for fully clamped thick plates with different geometric parameters subjected to both uniaxial and biaxial compressions, which are well validated by the available studies and refined FEA. Besides helping one to pursue more analytic solutions of the plate and shell problems, the present method is also expected to serve as a benchmark approach for examining the accuracy of other numerical methods.

Acknowledgements The authors gratefully acknowledge the support from the Young Elite Scientists Sponsorship Program by CAST (No. 2015QNRC001), Opening Fund of State Key Laboratory of Nonlinear Mechanics, Chinese Academy of Sciences, and Fundamental Research Funds for the Central Universities of China (No. DUT18GF101).

Appendix A: Definition of double finite integral transforms

The following double finite integral transforms are used for W, φ_x and φ_y:

$$W^{\mathrm{ss}} = \int_0^a \int_0^b W(x,y)\sin(\alpha_m x)\sin(\beta_n y)\mathrm{d}x\mathrm{d}y$$

$$\varphi_x^{\mathrm{cs}} = \int_0^a \int_0^b \varphi_x(x,y)\cos(\alpha_m x)\sin(\beta_n y)\mathrm{d}x\mathrm{d}y$$

$$\varphi_y^{\mathrm{sc}} = \int_0^a \int_0^b \varphi_y(x,y)\sin(\alpha_m x)\cos(\beta_n y)\mathrm{d}x\mathrm{d}y$$

where the superscripts "SS", "CS" and "SC" represent the double sine, cosine-sine and sine-cosine integral transforms with respect to variables x and y.

Appendix B: Matrix elements in Eq. (12)

$$
\begin{aligned}
T_{11} &= \frac{C\left[C + D\left(\alpha_m^2 + \beta_n^2\right)\right]}{\left[C + D\left(\alpha_m^2 + \beta_n^2\right)\right]\left[\alpha_m^2\left(C + N_x\right) + \beta_n^2\left(C + N_y\right)\right] - C^2\left(\alpha_m^2 + \beta_n^2\right)},\\
T_{12} &= -\frac{CD\alpha_m}{CN_x\alpha_m^2 + D\alpha_m^4\left(C + N_x\right) + \beta_n^2\left[CN_y + D\alpha_m^2\left(2C + N_x + N_y\right)\right] + D\beta_n^4\left(C + N_y\right)},\\
T_{13} &= -\frac{CD\beta_n}{CN_x\alpha_m^2 + D\alpha_m^4\left(C + N_x\right) + \beta_n^2\left[CN_y + D\left(2C + N_x + N_y\right)\alpha_m^2\right] + D\beta_n^4\left(C + N_y\right)},\\
T_{21} &= -\frac{C}{D}T_{12},\\
T_{22} &= -\frac{D\left\{\begin{array}{l}\alpha_m^2\left(C + N_x\right)\left[2C + D\alpha_m^2\left(1 - \mu\right)\right]\\ +\beta_n^2\left\{2CN_y + D\alpha_m^2\left[C\left(3 - \mu\right) + 2N_x + N_y\left(1 - \mu\right)\right]\right\} + 2D\beta_n^4\left(C + N_y\right)\end{array}\right\}}{\left[2C + D\left(1 - \mu\right)\left(\alpha_m^2 + \beta_n^2\right)\right]\left\{\begin{array}{l}CN_x\alpha_m^2 + D\alpha_m^4\left(C + N_x\right)\\ +\beta_n^2\left[CN_y + D\alpha_m^2\left(2C + N_x + N_y\right)\right] + D\beta_n^4\left(C + N_y\right)\end{array}\right\}},\\
T_{23} &= -\frac{D\alpha_m\beta_n\left\{2C^2 - D\left(1 + \mu\right)\left[\alpha_m^2\left(C + N_x\right) + \beta_n^2\left(C + N_y\right)\right]\right\}}{\left[2C + D\left(1 - \mu\right)\left(\alpha_m^2 + \beta_n^2\right)\right]\left\{\begin{array}{l}CN_x\alpha_m^2 + D\alpha_m^4\left(C + N_x\right)\\ +\beta_n^2\left[CN_y + D\alpha_m^2\left(2C + N_x + N_y\right)\right] + D\beta_n^4\left(C + N_y\right)\end{array}\right\}},\\
T_{31} &= -\frac{C}{D}T_{13},\\
T_{32} &= -T_{23},\\
T_{33} &= -\frac{D\left\{\begin{array}{l}2CN_x\alpha_m^2 + 2D\alpha_m^4\left(C + N_x\right)\\ +\beta_n^2\left\{2C\left(C + N_y\right) + D\alpha_m^2\left[C\left(3 - \mu\right) + N_x\left(1 - \mu\right) + 2N_y\right]\right\} + D\beta_n^4\left(1 - \mu\right)\left(C + N_y\right)\end{array}\right\}}{\left[2C + D\left(1 - \mu\right)\left(\alpha_m^2 + \beta_n^2\right)\right]\left\{\begin{array}{l}CN_x\alpha_m^2 + D\alpha_m^4\left(C + N_x\right)\\ +\beta_n^2\left[CN_y + D\alpha_m^2\left(2C + N_x + N_y\right)\right] + D\beta_n^4\left(C + N_y\right)\end{array}\right\}}.
\end{aligned}
$$

References

1. Kirchoff, G.: Uber das Gleichgewicht und die Bewegung einer elastischen Scheibe. J. Reine Angew. Math. (Crelle's J.) **40**, 51–88 (1850)
2. Reissner, E.: The Effect of Transverse Shear deformation on the bending of elastic plates. J. Appl. Mech. Trans. ASME **12**(2), A69–A77 (1945)
3. Mindlin, R.D.: Influence of rotatory inertia and shear on flexural motions of isotropic, elastic plates. J. Appl. Mech. Trans. ASME **18**(1), 31–38 (1951)
4. Srinivas, S., Rao, A.: Bending, vibration and buckling of simply supported thick orthotropic rectangular plates and laminates. Int. J. Solids Struct. **6**(11), 1463–1481 (1970)
5. Wang, C., Xiang, Y., Kitipornchai, S., Liew, K.: Buckling solutions for Mindlin plates of various shapes. Eng. Struct. **16**(2), 119–127 (1994)
6. Liew, K.: Solving the vibration of thick symmetric laminates by Reissner/Mindlin plate theory and thep-Ritz method. J. Sound Vib. **198**(3), 343–360 (1996)
7. Wang, C.M., Lim, G.T., Reddy, J.N., Lee, K.H.: Relationships between bending solutions of Reissner and Mindlin plate theories. Eng. Struct. **23**, 838–849 (2001)
8. Ghannadpour, S., Ovesy, H., Zia-Dehkordi, E.: Buckling and post-buckling behaviour of moderately thick plates using an exact finite strip. Comput. Struct. **147**, 172–180 (2015)
9. Jafari, N., Azhari, M.: Buckling of moderately thick arbitrarily shaped plates with intermediate point supports using a simple hp-cloud method. App. Math. Comput. **313**, 196–208 (2017)
10. Civalek, Ö.: Three-dimensional vibration, buckling and bending analyses of thick rectangular plates based on discrete singular convolution method. Int. J. Mech. Sci. **49**(6), 752–765 (2007)
11. Bui, T., Nguyen, M., Zhang, C.: Buckling analysis of Reissner-Mindlin plates subjected to in-plane edge loads using a shear-locking-free and meshfree method. Eng. Anal. Bound. Elements **35**(9), 1038–1053 (2011)

12. Bodaghi, M., Saidi, A.R.: Thermoelastic buckling behavior of thick functionally graded rectangular plates. Arch. Appl. Mech. **81**(11), 1555–1572 (2011)
13. Nazarimofrad, E., Zahrai, S.M., Kholerdi, S.E.S.: Effect of rotationally restrained and Pasternak foundation on buckling of an orthotropic rectangular Mindlin plate. Mech. Adv. Mater. Struct. **25**(7), 592–599 (2018)
14. Yiotis, A.J., Katsikadelis, J.T.: Buckling analysis of thick plates on biparametric elastic foundation: a MAEM solution. Arch. Appl. Mech. **88**(1–2), 83–95 (2018)
15. Li, R., Ni, X., Cheng, G.: Symplectic superposition method for benchmark flexure solutions for rectangular thick plates. J. Eng. Mech. **141**(2), 04014119 (2015)
16. Li, R., Wang, P., Tian, Y., Wang, B., Li, G.: A unified analytic solution approach to static bending and free vibration problems of rectangular thin plates. Sci. Rep. **5**, 17054 (2015)
17. Li, R., Zheng, X., Wang, H., Xiong, S., Yan, K., Li, P.: New analytic buckling solutions of rectangular thin plates with all edges free. Int. J. Mech. Sci. **144**, 67–73 (2018)
18. Yao, W., Zhong, W., Lim, C.W.: Symplectic Elasticity. World Scientific, Singapore (2009)
19. Lim, C.W., Lu, C.F., Xiang, Y., Yao, W.: On new symplectic elasticity approach for exact free vibration solutions of rectangular Kirchhoff plates. Int. J. Eng. Sci. **47**(1), 131–140 (2009)
20. Lim, C.W.: Symplectic elasticity approach for free vibration of rectangular plates. Adv. Vib. Eng. **9**(2), 159–163 (2010)
21. Lim, C.W., Xu, X.S.: Symplectic elasticity: theory and applications. Appl. Mech. Rev. **63**(5), 050802 (2010)
22. Li, R., Zhong, Y., Tian, B., Liu, Y.: On the finite integral transform method for exact bending solutions of fully clamped orthotropic rectangular thin plates. Appl. Math. Lett. **22**(12), 1821–1827 (2009)
23. Tian, B., Li, R., Zhong, Y.: Integral transform solutions to the bending problems of moderately thick rectangular plates with all edges free resting on elastic foundations. Appl. Math. Model. **39**(1), 128–136 (2015)
24. Zhang, S., Xu, L., Li, R.: New exact series solutions for transverse vibration of rotationally-restrained orthotropic plates. Appl. Math. Model. **65**, 348–360 (2019)
25. Nwoji, C.U., Onah, H.N., Mama, B.O., Ike, C.C., Ikwueze, E.U.: Elastic buckling analysis of simply supported thin plates using the double finite Fourier sine integral transform method. Explor. J. Eng. Technol. **1**(1), 37–47 (2017)
26. Mama, B.O., Nwoji, C.U., Ike, C.C., Onah, H.N.: Analysis of simply supported rectangular Kirchhoff plates by the finite Fourier sine transform method. Int. J. Adv. Eng. Res. Sci. **4**(3), 285–291 (2017)
27. Xing, Y., Xiang, W.: Closed-form solutions for eigenbuckling of rectangular Mindlin plate. Int. J. Struct. Stab. Dyn. **16**(8), 1550079 (2016)
28. ABAQUS: Analysis User's Guide V6.13. Dassault Systèmes, Pawtucket (2013)
29. Teo, T., Liew, K.: A differential quadrature procedure for three-dimensional buckling analysis of rectangular plates. Int. J. Solids Struct. **36**(8), 1149–1168 (1999)
30. Xiang, Y.: Numerical developments in solving the buckling and vibration of Mindlin plates. Ph.D. Thesis, The University of Queensland, Australia (1993)